Periodicities in fair weather potential gradient data from multiple stations at different latitudes

Atmospheric Research 276 (2022) 106250

Contents lists available at ScienceDirect

Atmospheric Research

journal homepage: www.elsevier.com/locate/atmosres

Periodicities in fair weather potential gradient data from multiple stations at different latitudes

J. Tacza [a,b,*], K.A. Nicoll [c], E. Macotela [d,e]

[a] Institute of Geophysics, Polish Academy of Sciences, Warsaw, Poland
[b] Center of Radio Astronomy and Astrophysics Mackenzie, Engineering School, Mackenzie Presbyterian University, Sao Paulo, Brazil
[c] Department of Meteorology, University of Reading, UK
[d] Faculty of Mathematics and Natural Sciences, University of Rostock, Rostock, Germany
[e] The Leibniz Institute of Atmospheric Physics at the University of Rostock, Kuhlungsborn, Germany

ARTICLE INFO

Keywords:
Atmospheric electricity
Global electric circuit
Space weather
Lomb-Scargle periodogram
Wavelet transform

ABSTRACT

Analysis of the variation of the potential gradient (PG) at ground level is important to monitor the global electric circuit and the different solar and geophysical phenomena affecting it. However, this is challenging since several local factors (e.g., meteorological) produce perturbations in the potential gradient. Time series and spectral analysis of PG at several stations can help to minimise local effects so that global effects may be more clearly observed. In this work, for the first time we performed spectral analysis of the potential gradient recorded at several sites located at Vostok, Concordia, Halley and Casleo (Southern Hemisphere), and Sodankyla and Reading (Northern Hemisphere). In order to find the main periodicities and how the amplitude of those periods change as a function of time we use the Lomb-Scargle periodogram and the wavelet transform, respectively. For all PG sites we found periodicities of 0.5-, 1-, ~180- and 365-day. Our results show that the 0.5-day (1-day) periodicity is more prominent during the months of June–July-August (December–January-February). Evidence of ~27- and ~ 45-day periods was also observed at multiple sites. Further analysis using the cross-wavelet transform for PG versus cosmic rays, PG versus Madden-Julian Oscillation index, and PG versus meteorological parameters, show clues that the 27- and 45-day periods are likely related to the solar rotation and Madden-Julian Oscillation, respectively. Furthermore, our results show that during the passages of co-rotating interaction regions, the 27-day period for PG vs cosmic rays XWT is stronger than for the other XWT analysis.

1. Introduction

The atmospheric electric field (or potential gradient, PG) is the most widely measured parameter in atmospheric electricity research, and results from vertical separation of charge in the global electric circuit (GEC). In fair weather conditions the PG is positive and typically around 100 V/m (Harrison, 2013), and is generally measured by a sensor known as an electric field mill. At any given measurement site, PG is influenced by a number of local and global factors. Local factors include the effect of meteorological parameters such as wind, precipitation, fog, convective activity, and changes in aerosol properties (e.g., from pollution or dust) (Harrison and Nicoll, 2018). The magnitude of the effect of such local influences on PG vary depending on the type of measurement site and location, e.g., a desert site in an arid location would expect to see large influences on PG from convective activity and varying dust concentration, whereas a mid latitude site in a rural location on a grass covered field may be mostly influenced by the occurrence of precipitation events (e.g., Nicoll et al., 2019). When these local effects are minimal (or negligible) on PG, it is possible to observe the influence of global effects, such as the GEC. It is well established that Earth has a GEC through which charge separation in thunderstorms sustains large-scale current flow around the planet (Wilson, 1921). Study of the GEC is an active area of research due to its dependence on thunderstorm and lightning activity, particularly in regard as to how these will vary under a changing climate (e.g., Price, 2009; Aich et al., 2018; Holzworth et al., 2021). Another area of current research in atmospheric electricity is the role that atmospheric electricity plays in modulating cloud properties and therefore Earth's radiative balance (Tinsley, 2008; Nicoll and Harrison, 2016; Harrison et al., 2020). One of the most uncertain elements of this is the effect of space weather influences on atmospheric

* Corresponding author at: Institute of Geophysics, Polish Academy of Sciences, Warsaw, Poland.
E-mail address: josect1986@gmail.com (J. Tacza).

https://doi.org/10.1016/j.atmosres.2022.106250
Received 2 February 2022; Received in revised form 9 April 2022; Accepted 13 May 2022
Available online 18 May 2022

electricity through changes in cosmic ray ionisation from solar flares and energetic particle events. Analysis of energetic particle data, solar data and simultaneously measured atmospheric electricity data (including PG) from multiple sites, using a variety of sophisticated data analysis techniques is likely required to understand these complex relationships.

An underused technique that can be employed to investigate local, global and solar influences on PG is spectral analysis. This provides a way to measure the strength of periodic components of a PG time series at different frequencies. The time evolution of these characteristic periodic components/frequencies can then be investigated using a technique known as wavelet analysis. Although use of spectral analysis techniques on PG data has been reported previously in the literature, this is almost always only performed on PG data from individual measurement sites (e.g., Harrison and Märcz, 2007), and is often used alongside other data analysis techniques to investigate the influence of specific physical processes on PG data. In this paper we focus entirely on the application of spectral analysis techniques to a variety of different PG datasets from widely spaced locations. The aim of this is to assess the importance of different physical processes on PG at different types of measurement sites, as well as investigate solar effects on PG as a function of time and latitude.

Previous Atmospheric Electric (AE) studies which have employed spectral analysis techniques have investigated phenomena at characteristic time scales ranging from fractions of a second (e.g., turbulence) to years (e.g., solar variations). Studies on spectral relationships between turbulence and AE parameters include those by Oluwafemi et al. (1974), Israelsson and Oluwafemi (1975); Makhdoomi and Raina (1988); Anisimov et al. (2002); Anisimov et al. (2014); and Conceição et al. (2018). Other short term influences on AE parameters investigated by spectral techniques include sea breeze effects (Trevitt, 1984), periodicities related to earthquake precursors (Mikhailov et al., 2004), and desert dust events (Silva et al., 2016).

Of the studies investigating longer term periodicities in AE data, the following periodicities are typically reported: 0.5-day, 1-day, 7-day, 27-day, 365-day and 1.68-year. The 0.5- and 1-day periodicities are typically attributed to the repeatable diurnal variation in PG from local and GEC sources. The 1-day periodicity tends to be more often observed than the 0.5-day periodicity. For instance, Xu et al. (2013) and Tacza et al. (2021a) observe 1-day periodicities in PG at Tibet and Argentina respectively, but not the 0.5-day. A 7-day periodicity has been observed at urban sites (e.g., in Lisbon, Portugal (Silva et al., 2014); Panska Ves, Czech Republic (Chum et al., 2021)), and is thought to be related to variations in aerosol pollution between weekdays and weekends. The 27-day periodicity is often related to variations in solar activity, as the period of a typical solar rotation varies between 24 and 38 days (depending on solar latitude), but with an average of 27 days near the solar equator (Stenflo, 1990). Observations of 27-day periodicities in PG data in the literature are rare, but Harrison et al. (2011) reported evidence of this in PG data from Nagycenk, Hungary during 1996–1997. This period coincided with the occurrence of a coronal hole, which is known to increase the solar wind outflow and influence the formation of long-lived solar co-rotating interaction regions (CIRs). Such CIRs modulate cosmic ray fluxes (e.g., Rouillard et al., 2007), often producing very obvious periodic 27-day variations in surface neutron monitor data which are even observable by eye. Studying periods which are known to contain well defined solar-induced oscillations (such as CIRs) provides opportunities to investigate the effects of solar variability on AE variables and is discussed further in section 5 of this paper. A more recent publication by Chum et al. (2021) discusses a 25.7-day periodicity observed at two sites in the Czech Republic, using data from 2016 to 2019. This is consistent with the solar rotation period at low solar latitudes, and also with periodicities in the Vx component of the solar wind speed, and may be an indication that solar effects can be observed in surface AE measurements during periods which don't show strong solar-induced oscillations. Another periodicity that is thought to be related to solar variations is a 1.68 years oscillation, which has been observed in the very long time series of PG measurements from Nagycenk, Hungary (Harrison and Märcz, 2007; and Harrison et al., 2011) from 1978 to 1990. The same 1.68-year oscillation has been observed in surface neutron monitor data and previously identified as of heliospheric origin (Rouillard et al., 2007), thought to be related with coronal holes (with similar signals observed in Voyager spacecraft data (Kato et al., 2003)).

The aim of this paper is to apply spectral analysis techniques to near surface PG data from a variety of measurement sites from polar regions and mid latitude sites, in order to gain insights into the factors influencing PG at local and global scales. Special attention is paid to investigating solar influences on PG as these are one of the least well understood aspects of atmospheric electricity in current research. Section 2 introduces the PG datasets and section 3 explains the spectral analysis methods used in the paper. Section 4 shows periodograms from the measurement sites and investigates the effect of performing seasonal analysis with periodograms. Section 5 uses cross-wavelet transforms to compare power spectra from PG data with neutron monitor data (as a proxy for galactic cosmic ray ionisation) in order to study solar influences on atmospheric electricity as a function of time during the past two decades. The section concludes with an exploration of local meteorological and Madden-Julian Oscillation influences on the observed 27-day period. Section 6 and 7 includes the discussion and conclusions, respectively.

2. PG data sources

In this paper we deliberately select a number of PG measurement sites (six in total) located at different latitudes across both hemispheres. These locations are: Vostok (VOS), Concordia (CON), Halley (HAL), Sodankyla (SOD), Reading (REA) and Casleo (CAS), with details provided in Table 1. Previous PG studies have demonstrated that each of these sites exhibits global atmospheric electricity signals at least some of the time. Fig. 1 shows a map of the PG sites. Vostok and Concordia stations are located on the Antarctic Plateau, at high altitude (3488 and 3250 m a.s.l., respectively). The diurnal variations in PG from both sites have been shown to have good similarity with the 'universal' Carnegie curve (Burns et al., 2017), and many papers in the literature discuss details of these datasets (Burns et al., 2005; Burns et al., 2012; Burns et al., 2017). Halley station is also located in Antarctica, but at much lower altitude, on the Brunt Ice Shelf, approximately 50 km from the coast. Tacza et al. (2021b) discuss details of the Halley site and instrumentation. It is also important to study atmospheric electricity variations at high latitudes in the northern hemisphere, therefore Sodankyla (in the Arctic), is also included here (Tacza et al., 2021b). Finally, in order to study PG variations at lower latitudes Reading and Casleo stations are included, which are located in middle latitudes. Previous analysis of PG measurements from these stations have demonstrated global effects of the GEC in Fair Weather (FW) conditions (Harrison, 2013; Tacza et al., 2021a).

Fig. 2 shows a time series of hourly PG averages for each station (all PG values are included here and no selection is made for FW conditions as yet). Differences in the mean values, as well as variability in PG is observed between the different measurement stations, which is associated with the meteorological conditions at each location site, as well as the altitude, terrain, and surface land cover. For the PG stations located in the Antarctic (VOS, CON and HAL) the PG values from these sites are predominantly positive, which is likely associated with lack of rainfall (as almost all precipitation at these sites falls as snow). The high variability in PG at these sites is also likely related to transport of space charge from blowing snow, which occurs during high winds, and is most common during the winter months. The summer months in the Antarctic stations (December, January, February) show a clear decrease in variability compared to the other seasons. At the SOD site, the high variability is observed during the months of spring and summer when liquid precipitation is common. For REA, rainfall occurs all year round, but is most prevalent during the winter months, hence high variability is

Table 1
Details of the PG stations and their locations. FW PG range gives the range of values designated as fair weather, which is used in our data analysis.

Site	Coordinates /Altitude	Data Period	Missing data ratio (%)	Site Type	FW PG range (V/m)	Missing data ratio after applying FW criterion (%)
Vostok (VOS)	78.5°S, 107°E 3488 m	January 2006–December 2011 (6 years)	3	Antarctic Plateau, snow cover during whole year	100–300	30
Concordia (CON)	75.1°S, 123°E 3250 m	January 2009–December 2011 (3 years)	4	Antarctic Plateau, snow cover during whole year	200–800	21
Halley (HAL)	75.58°S, 26.66°W 30 m	February 2015–December 2016 (1.9 years)	8	Ice sheet, snow cover during whole year	30–150	38
Sodankyla (SOD)	67.37°N, 26.63°E 180 m	June 2017–June 2021 (4 years)	7	Forest, snow cover from October to May	10–150	15
Reading (REA)	51.44°N, 0.94°W 66 m	January 2007–December 2017 (11 years)	4	Urban, grass covered	50–200	26
Casleo (CAS)	31.8°S, 69.29°W 2480 m	January 2010–April 2021 (11.3 years)	10	High mountain, some low bushes	20–150	14

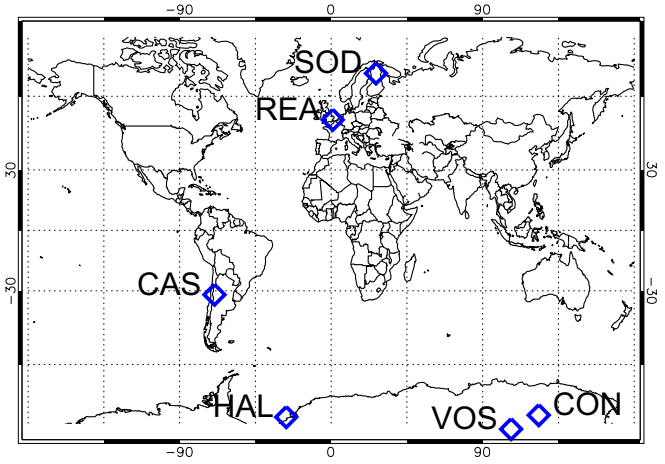

Fig. 1. Map with the location of PG measurement sites discussed in the paper.

present for most of the year. For CAS site there is a clear seasonal dependence in the PG values which is associated with the prevalence of thunderstorms during the southern hemisphere summer months of December, January and February.

For this work, it is important to minimise the effects of local influences on the PG so that global influences may be more easily identified. We thus define a criterion for FW PG hours, which is based on the PG histogram for each site. The histograms are shown in Fig. 3 for each of the six sites. As mentioned in the previous section, it is expected that the magnitude of the PG values differs between sites as a result of the altitude of the site, the surrounding terrain and surface type, as well as the height of the electric field mill above the surface. We make no attempt here to standardise the PG values (e.g., to reduce them all to the PG value on a flat area at ground level), as this particular study is primarily concerned with spectral analysis, so absolute magnitudes of PG are not important. Additionally, we did not correct the influence of the polar cap ionospheric potential at VOS and CON sites (Burns et al., 2017), since our purpose is to find if there is any latitude dependence of the PG periodicities, especially solar related periodicities.

To select FW PG hours we use only the PG data itself, based on the histograms shown in Fig. 3. This follows a similar technique described in previous reports (e.g., Nicoll et al., 2019 where only PG values in the inner 80% of the distribution were considered, i.e. 10th–90th percentiles). Here we employ a slightly different percentile selection for each site to ensure that non FW data (e.g, negative and very large PG values) are removed as much as possible. As such the following FW PG ranges were selected for each site: VOS (100-300 V/m, corresponding to the 3–70 percentiles), CON (200-800 V/m, 2–80%), HAL (30-150 V/m, 5–70%), SOD (10-150 V/m, 5–90%), REA (50-200 V/m, 20–90%) and CAS (20-150 V/m, 2–90%). With this criterion we take advantage of removing the outliers (due to non-FW PG data, e.g. thunderstorms) and minimise the data gaps (which will be greater if we use a meteorological criterion). Table 1 summarizes the coordinates, data period, missing data rate, site type, the FW PG range chosen for each of the six PG stations and the missing data rate after applying the FW criterion.

3. Data analysis methods

As stated in the introduction, the main aim of this paper is to use a variety of spectral analysis techniques to investigate common factors influencing PG at a variety of different measurement sites over a range of latitudes. In this section we describe the various techniques used to perform the spectral analysis in this paper. For this we used the Lomb-Scargle periodogram and the wavelet transform, since these techniques have proved to be useful for the PG analysis in the literature.

3.1. Lomb–Scargle periodogram

The Lomb–Scargle (LS) periodogram (Lomb, 1976; Scargle, 1982) is a commonly used statistical tool that allows efficient computation of a Fourier-like power spectrum estimator for unevenly sampled time-series (Press and Rybicki, 1989). This is precisely the characteristics of our PG measurements after the fair-weather criterion has been applied. The LS periodogram offers an intuitive means of determining the period of any recurring oscillations in a dataset and has often been used in atmospheric electricity analysis (e.g., Harrison et al., 2011; Silva et al., 2014).

3.2. Wavelet analysis

Wavelet analysis is a tool that decomposes a time series into the time–frequency domain, making it possible to determine both the dominant modes of oscillation (wavelets) and how those modes vary with time (Torrence and Compo, 1998). In this study a Morlet function (Morlet et al., 1982) with frequency $w_0 = 6$ is used to extract the dominant modes. This wavelet function provides a good balance between time and frequency localization (Grinsted et al., 2004). The wavelet technique demands constant time steps between samples, however, as explained in section 3.1 this is not the case for our PG observations. To allow the wavelet computation, those gaps were filled by using their respective smoothed values with a 2-year moving average. As shown by Macotela et al. (2019) and Tacza et al. (2021b), this procedure has the advantage of minimizing the introduction of artifacts in the wavelet analysis, especially at periods below 2 years.

In order to examine the relationship in the time-frequency domain of PG with cosmic-ray neutron, and PG with other parameters (e.g., meteorological time parameters), this study employs the cross-wavelet transform (XWT) toolbox for MATLAB package provided by Grinsted et al. (2004). The XWT is constructed from two continuous wavelet

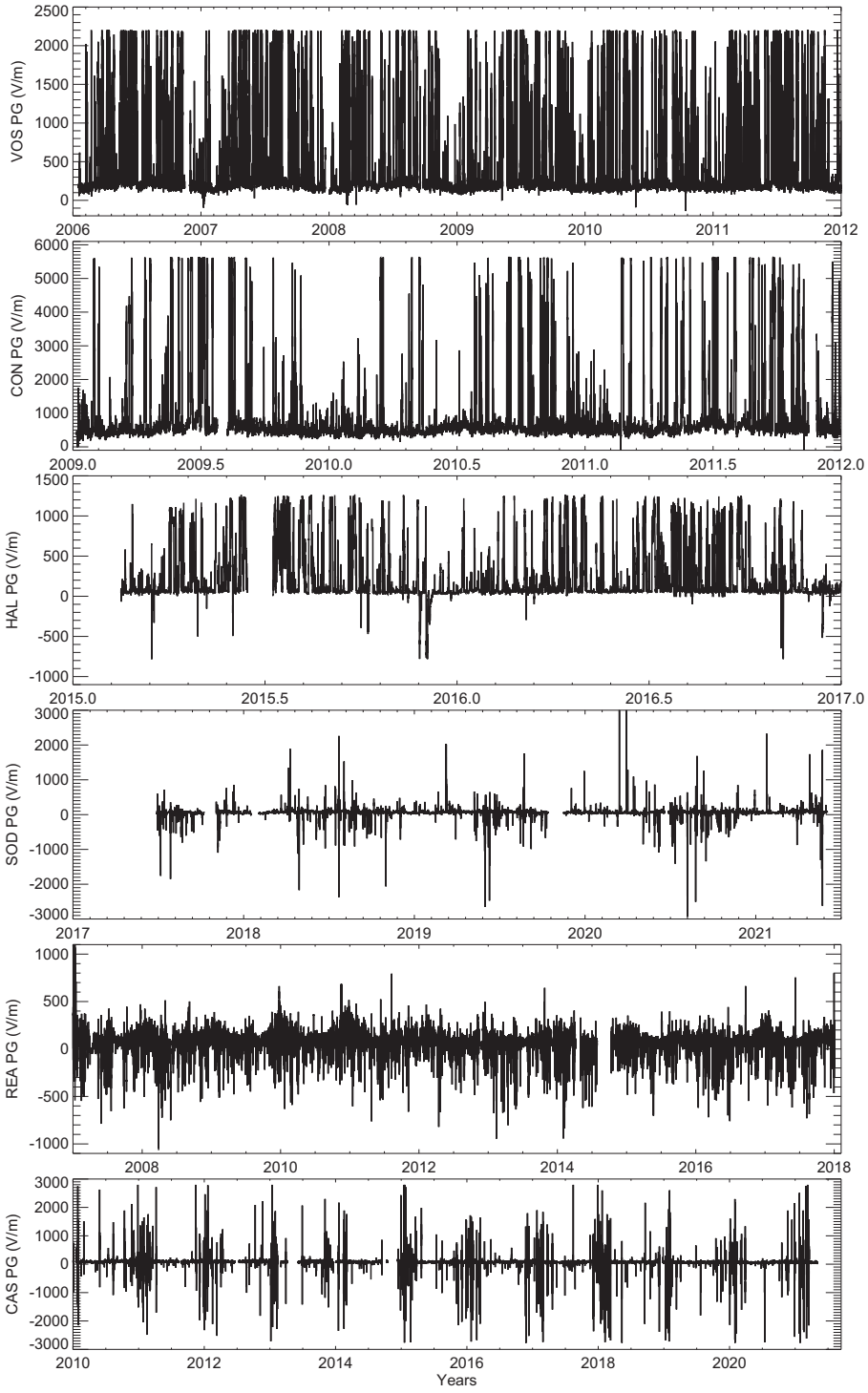

Fig. 2. Time series of PG hourly data for each site.

transforms (CWT), one for each parameter, and can be employed to find regions in the time-frequency domain where the two CWT show common changes in power. Another useful computation is the Global XWT power spectrum, which is calculated by averaging in time the XWT power spectrum ($\langle|XWT|\rangle$), to determine the significant periods in the whole time series of analysis. In the present study, each period of both the XWT distribution and the global XWT is corrected by its scale. This correction is employed to rectify the wavelet spectrum, which is biased in favor of larger periods (Liu et al., 2007).

4. PG periodicities

Fig. 4 shows the Lomb-Scargle periodogram of the PG time series for each site. Note that the X and Y axis are in log scale. The red vertical dashed lines indicate the 0.5-, 1-, 27-, 180- and 365-day periodicities, which are often the most commonly observed periodicities in PG data. Here we discuss evidence for each of these periodicities at the various sites, and provide a discussion as to their origins.

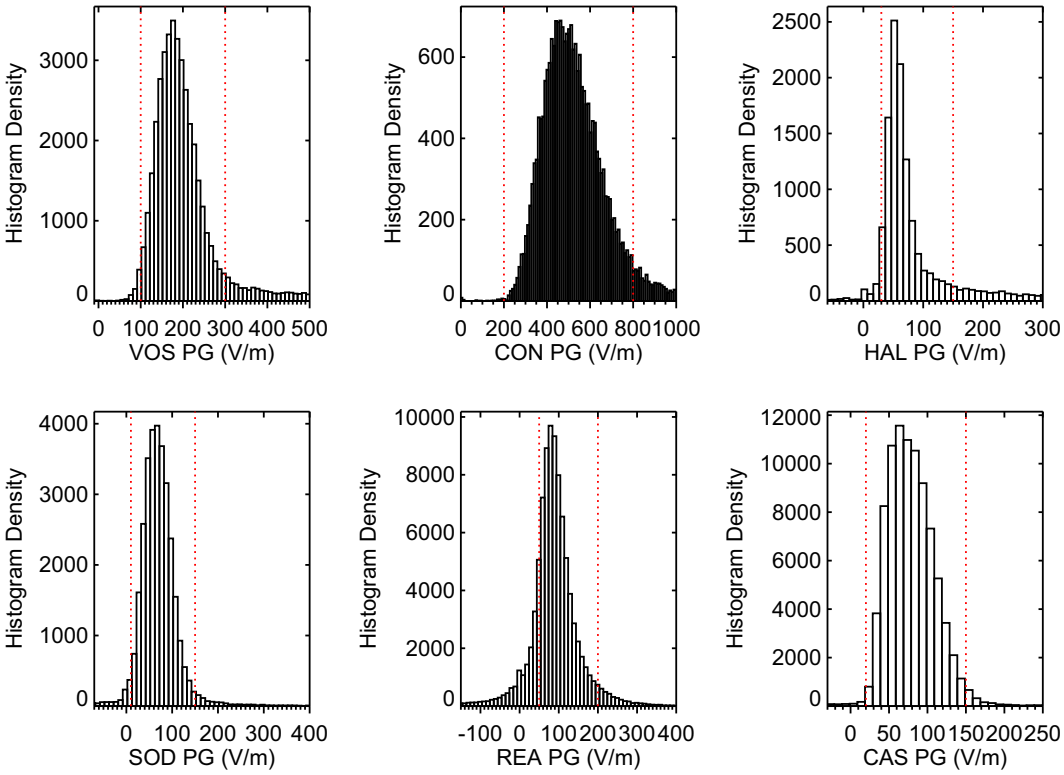

Fig. 3. Histograms of PG distributions from PG measurement sites. The range of PG values is restricted in the plots for easier visualization. Red vertical dashed lines indicate the FW PG ranges chosen for each site. The methodology to select the PG ranges is detailed in the main text. (For interpretation of the references to colour in this figure legend, the reader is referred to the web version of this article.)

4.1. Daily cycle: 0.5- and 1-day periodicity

The periods of 0.5-, and 1-day are clearly observed in PG at all stations from the LS periodograms shown in Fig. 4. These are the most common periodicities observed in PG measurements and are related to a combination of repeatable local and global influences. The 1-day periodicity is normally attributed to the GEC diurnal variation (i.e., Carnegie curve) which results from the diurnal cycle in global thunderstorms and electrified shower clouds, with a single maxima at 19UT (due to the peak in convective activity over the American continents). Previous work (e.g., Burns et al., 2017; Tacza et al., 2021a; Tacza et al., 2021b) has shown evidence of Carnegie-like diurnal variations in PG at all of these sites, therefore it is expected that the 1-day periodicity be observed at these sites. The 0.5-day periodicity can also be related to the GEC diurnal variation, through a second, and much smaller, morning peak (around 09UT) which is typically associated with Australian/Asian convective activity (e.g., as observed at VOS and CON (Burns et al., 2017)). Additionally, the 0.5-day period can be affected by secondary peaks in the PG diurnal variation often related to more local short term meteorological influences (such as a secondary peak observed in the diurnal variation curve in the morning due to local aerosol effects, convection influences, and the sunrise effect). It is interesting to note that at all of the sites (except REA), the 1-day periodicity peak is larger than the 0.5-day peak, which suggests that the GEC influence dominates over the local influences during the FW periods considered here.

In order to investigate the 0.5- and 1-day periodicities further, it is possible to separate the PG time series according to seasons. We know that at many of the sites, the local influences on PG vary according to season, therefore it is of interest to investigate whether anything can be learned about the dominance of the local versus global influences on PG purely by using spectral analysis techniques. Since we are analysing sites located in opposite hemispheres we must be cautious about this: REA and SOD are in the northern hemisphere, where it is summer in June–July-August (but winter for VOS, CON, HAL, and CAS which are in the southern hemisphere). Fig. 5 shows the Lomb-Scargle periodogram of the PG values separated for the months of December–January-February (DJF, red) and June–July-August (JJA, black). Focusing on the 0.5-day periodicity first, it is observed that the 0.5-day periodicity is more intense during JJA months (black) compared to the 1-day periodicity at all sites (with the exception of the CAS site). This may be related to the double maximum peak (i.e., at 09UT and 19UT) which is often attributed to GEC influences. This is observed at VOS, CON and in the Carnegie curve (Burns et al., 2017), with the secondary morning peak at 09UT being stronger during JJA than DJF. Previous analysis of PG at REA (e.g., Nicoll et al., 2019), and SOD (Tacza et al., 2021b) shows the existence of a clear seasonal cycle in PG, with a double diurnal peak in the summer (JJA), but single diurnal peak in the winter months (DJF). This is consistent with the LS Periodogram in Fig. 5, which shows that the 0.5-day periodicity (which would represent a double peak in the diurnal cycle) is stronger at both sites during local summer (JJA) than winter (DJF). Since REA is an urban site it makes sense that this should be more influenced by seasonal variations in local aerosol sources than most of the Antarctic sites (which are generally very clean air sites), and the increased morning peak at REA in JJA is most likely linked to a combination of local convective activity and aerosol pollution.

Focusing on the 1-day periodicity now, Fig. 5 shows that this is more intense during the months of DJF for all sites. This is consistent with the discussion in the previous paragraph, which explains that for REA and SOD, a single maxima diurnal variation in PG dominates in DJF, and also for VOS, HAL, and CON (where it is local summer and so local meteorological influences are smaller, and GEC influences are more apparent).

4.2. Monthly cycle - 27 day periodicity

Previous studies have occasionally found evidence of a periodicity around 27 days in surface PG measurements (e.g., Harrison et al., 2011;

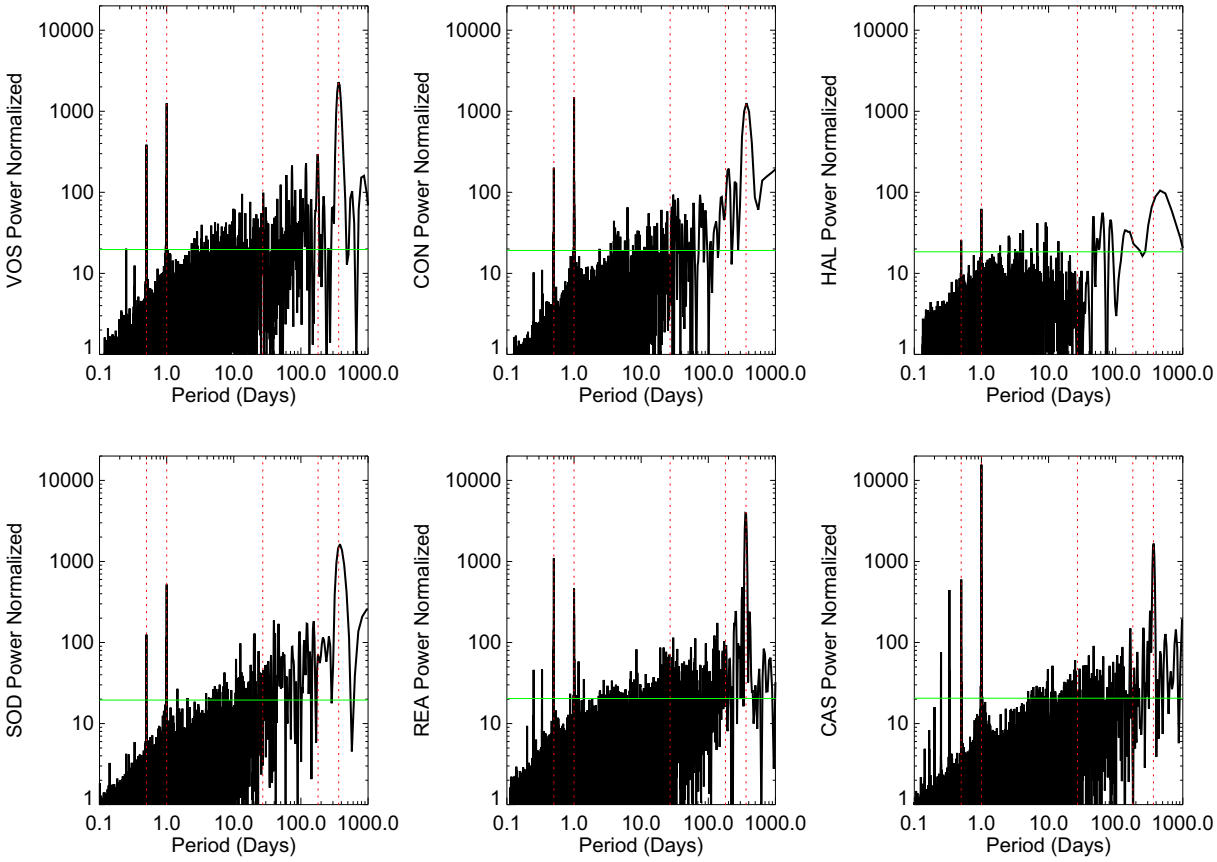

Fig. 4. Lomb-Scargle periodograms for PG hourly values from all measurement sites. X and Y axes are in log scale and the red vertical dashed lines indicate 0.5-, 1-, 27-, 180- and 365-day periodicities, respectively. The green horizontal lines indicate the false alarm probability level of 0.0001 (99.99% confidence interval). (For interpretation of the references to colour in this figure legend, the reader is referred to the web version of this article.)

Chum et al., 2021) which is thought to be related to solar activity. This arises from the approximately 27-day solar rotation period, which modulates the galactic cosmic ray flux (GCR) on similar timescales. Since ionisation from GCRs is the main source of ionisation in the atmosphere above a height of 1 km, it follows that we would expect a modulation of the near surface PG on similar timescales. Other solar related periodicities have also been observed at 9 and 13.5 days, which are harmonics of the solar rotation period (Sabbah and Kudela, 2011). Such periodicities have been reported in Interplanetary Magnetic Field (IMF) data, solar wind speed, and also neutron monitors which detect the nucleonic component of Galactic Cosmic Rays (GCRs) (Singh et al., 2012). The 9-, 13.5- and 27-day periodicities are seldom observed in PG data, however, as they are often masked by other local effects on PG. Examination of Fig. 4 does not show clear evidence of a periodicity around 27 days for any of the sites, possibly because this is swamped by signals from stronger, more intense periodicities. We therefore plot an additional LS periodogram (Fig. 6) which focuses on periods between 5 and 100 days, in order to exclude the strongest periodicities at 0.5, 1 and 365 days. Red vertical dashed lines in Fig. 6 indicate 9-, 13- and 27-day periodicities. The 27-day periodicity is clearly observed at VOS, and some evidence of periodicities around 27 days is found in CON (~30 days), REA (~30 days) and CAS (~25 days). The 9-day periodicity is observed at all three of the Antarctic sites VOS, CON, HAL, with some evidence of a broader peak (9-11 days) at REA and CAS. The 13-day periodicity is observed at VOS, CON and SOD. A summary of the various periodicities and the sites that they appear at is given in Table 2. Although there is support for the idea that the solar periodicities are more strongly observed at high latitude sites from Fig. 6 (which we would expect as solar influences are strongest in the polar regions), this is not entirely the case. SOD, which is at high latitudes in the northern hemisphere only shows a 13-day periodicity, and REA (which is a mid-latitude site) shows a strong 9-day periodicity, as well as a broad peak around 30 days. It is possible that other influences rather than solar ones are responsible for such peaks, thus further investigation of the periodicities around the 27-day timescale is performed in section 5 of this paper.

Fig. 6 also demonstrates some additional, longer term periodicities at some of the sites, specifically, around 44 days and 52 days (shown by blue vertical dashed lines). Tacza et al. (2021b) reported a 44-day periodicity at SOD, which is also shown to be strongly present here at VOS. HAL exhibits a 52-day periodicity, again also present at VOS from Fig. 6. Some evidence of these periodicities are also observed in REA and CAS. The origin of these periodicities is uncertain, but one possibility could be the influence from the Madden-Julian Oscillation (MJO). This will be discussed further in the next section.

4.3. Semi annual and annual oscillations: 180- and 365-day periodicity

The existence of a 365-day periodicity in PG data can be expected due to an annual cycle in the GEC, as well as local meteorological variables. For example, most sites will experience an annual cycle in convective processes (which tend to maximise in local summer, and minimise in winter); rainfall; and, at high latitude sites, wind speed (which generates substantial space charge and large PG values due to blowing snow). This 365-day periodicity can be even observed by eye at some measurement sites (e.g., Fig. 2 shows very strong annual cycles at CAS and VOS). Fig. 4 demonstrates a strong 365-day periodicity at all of the sites studied here, with the exception of Halley, but this is expected as only 2 years of data are studied. A further 180-day periodicity is also observed at VOS and CON, with some evidence of it present at the other

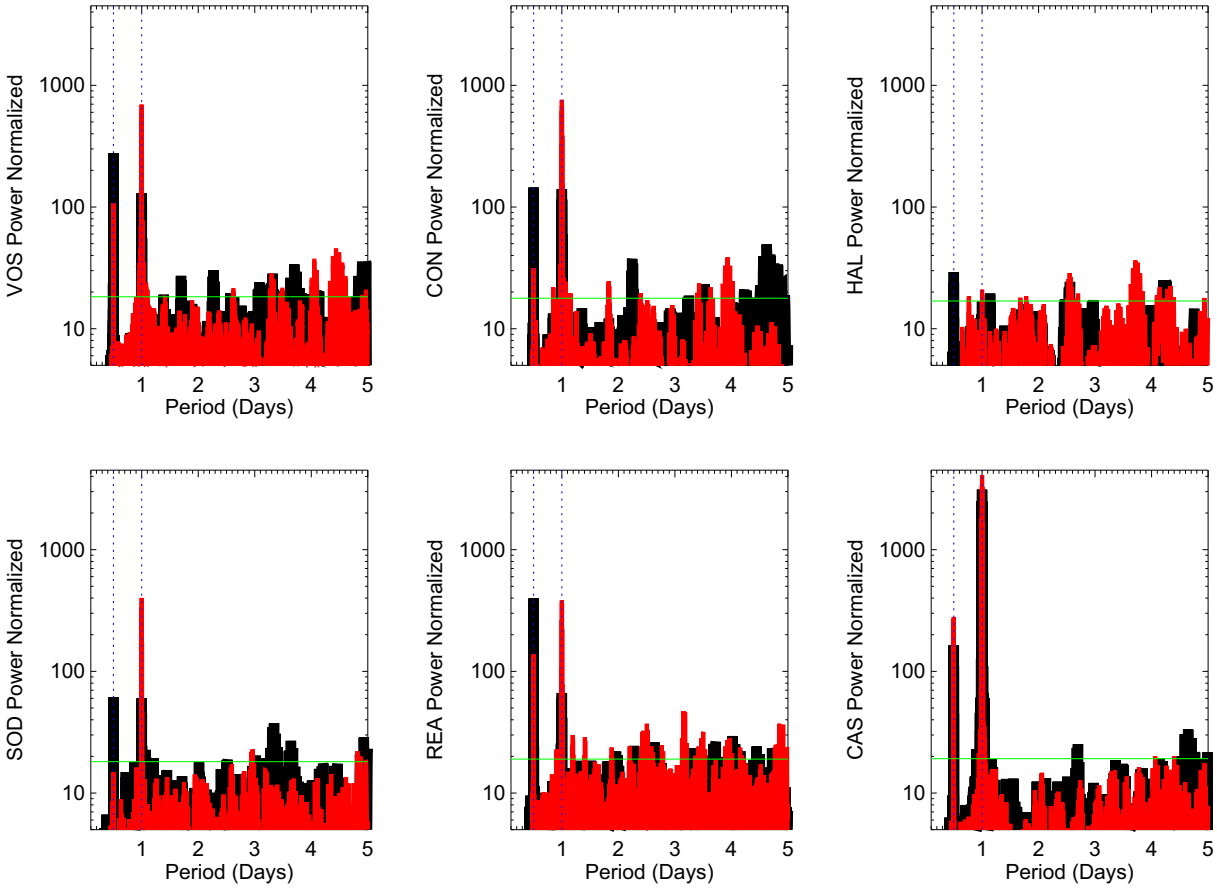

Fig. 5. Lomb-Scargle periodograms for each of the PG measurement sites plotted separately for the months of December–January-February (DJF, red) and June–July-August (JJA, black). The blue vertical dashed lines indicate the 0.5- and 1-day periodicities. The green horizontal lines indicate the false alarm probability level of 0.0001 (99.99% confidence interval). (For interpretation of the references to colour in this figure legend, the reader is referred to the web version of this article.)

sites, but it is not strongly observed. Besides terrestrial effects, the 180-day periodicity could be additionally affected by extraterrestrial factors. For example, Silva and Lopes (2017) reported evidence of periodicities between 150 and 300 days in three different parameters: sunspot area, NM count rate and PG measurements. The authors suggested that these periods were associated with the Rieger-type periodicities (Rieger et al., 1984). These periodicities have been found in several solar parameters, e.g., indicators of solar magnetic activity, sunspot group number, but the physical reason for its occurrence is still not clear (Gurgenashvili et al., 2016 and references therein). Silva and Lopes (2017) suggested a possible influence of the solar magnetic activity (Rieger-type periodicities) in the neutron count rate and the PG. Recently, Jeong and Oh (2022) found a semi-annual variation in the time-series of 16 NM from 1964 to 2020. The authors associated this variation to a combination of terrestrial and extraterrestrial effects.

5. Solar periodicities in PG data

The Lomb-Scargle periodogram is one way of performing spectral analysis on PG datasets but it doesn't give any information about the strength of periodicities in a temporal sense. This is important when analysing atmospheric electricity data, as physical processes which influence PG may only be present during certain years. This is known to be the case for certain types of solar influences on atmospheric electricity, which will be investigated further here using wavelet analysis techniques. One way of investigating whether relationships exist between PG and solar activity is to perform cross-wavelet transforms (XWT) (as described in section 3.2), between PG and neutron monitor (NM) data. XWT is used to investigate regions in the time-frequency domain where the two time series show common changes in power. NM ground-based data is used because the monitors detect secondary nucleons produced by the interaction of the primary cosmic rays with the Earth's atmosphere. Observations showed that the NM count rate is better correlated with the maximum ionisation rate produced by the cosmic rays at ~15–20 km, known as the Regener-Pfotzer maximum (Regener and Pfotzer, 1935; Bazilevskaya et al., 2008; Harrison et al., 2014). The 9-, 13.5- and 27-day solar periodicities discussed in section 4 have been observed in NM data (Sabbah and Kudela, 2011) and the strength of these periodicities are known to vary in time, depending on solar activity and features on the surface of the sun.

Fig. 7 shows the daily sunspot number evolution (top panel) applying a moving average with a time window of 121 days. The sunspot number gives an indication of the solar cycle progression. This figure also shows the XWT distribution between PG and neutron monitor (NM) data. The colors indicate the common power of the two CWT examined, one for PG and the other for NM, ranging from low (blueish) to high (reddish). The cone of influence, which indicates the regions in time and frequency potentially influenced by edge effects, is not displayed since it is only important at periods higher than the ones shown here. For NM data we chose the nearest station to each PG site. In this way, we calculated the XWT between i) VOS, CON, HAL PG and McMurdo NM, ii) SOD, REA PG and Oulu NM, and iii) CAS PG and Athens NM for their corresponding time windows. Athens NM is not near to the CAS site but is approximately located in the same latitude but in the Northern Hemisphere (37°N). The datasets span two intervals of solar minimum (where sunspot number is small), and one solar maximum (where the sunspot

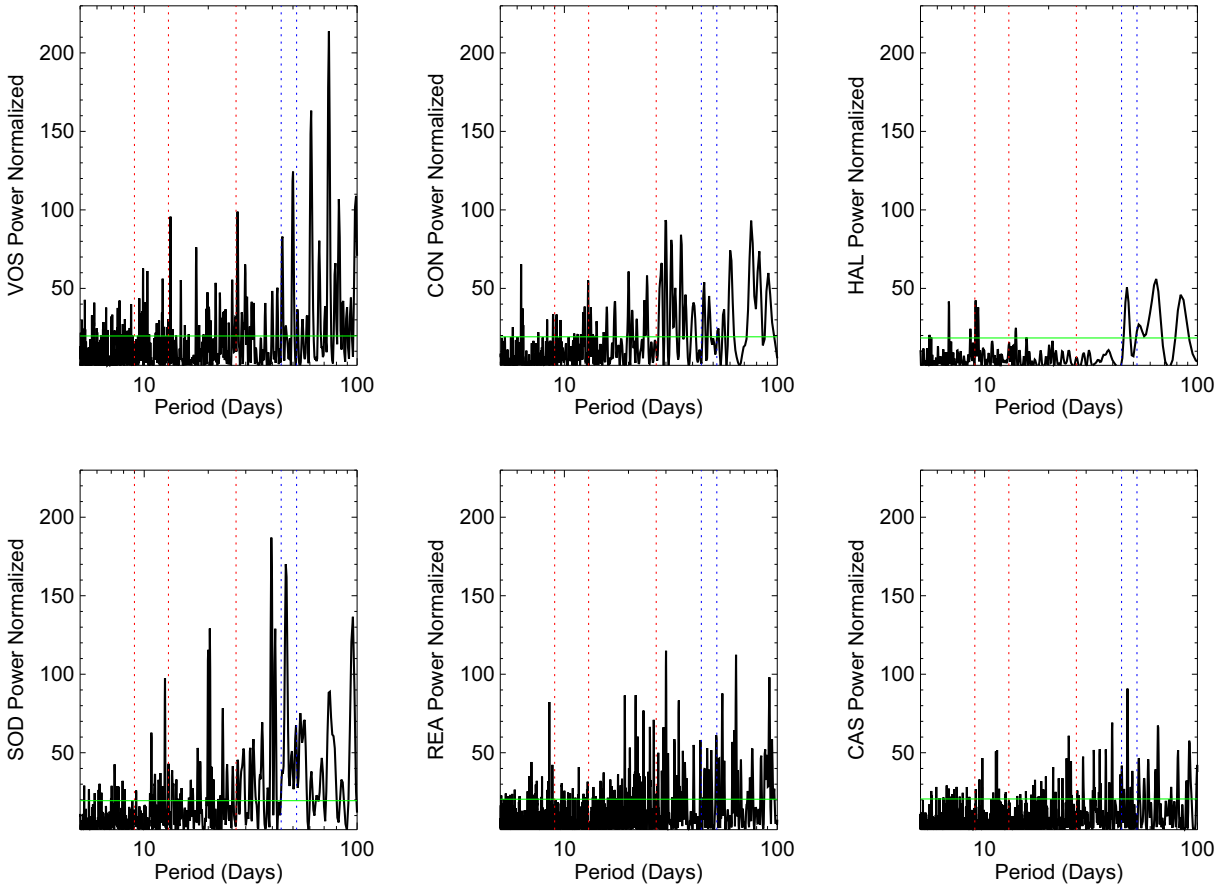

Fig. 6. Lomb-Scargle periodograms for FW PG from all measurement sites. The X axis is in log scale and the vertical dashed lines indicate 9-, 13-, 27- (red), 44- and 52- (blue) day periodicities respectively. The green horizontal lines indicate the false alarm probability level of 0.0001 (99.99% confidence interval). (For interpretation of the references to colour in this figure legend, the reader is referred to the web version of this article.)

Table 2
Summary of the periodicities observed at each site (✓) and also their closest periodicities. The dashed symbol (–) indicates that the periodicity is not observed at all.

	Period (days)							
Site	0.5	1	9	13	27	44–52	180	365
VOS	✓	✓	✓	✓	✓	✓	✓	✓
CON	✓	✓	✓	✓	~30d	–	✓	✓
HAL	✓	✓	✓	–	–	✓	✓	✓
SOD	✓	✓	–	✓	–	✓	–	✓
REA	✓	✓	9–11	–	~30d	✓	–	✓
CAS	✓	✓	9–11	–	~25d	✓	✓	✓

number is large).

In Fig. 7, the XWT for VOS shows intermittent common power at ~27- and ~ 13.5-day periods between 2006 and 2009, and again from 2011 to 2012. Similar behavior is observed for CON with an enhancement after 2011. For HAL, common powers are observed throughout the time window and are particularly stronger around the 13.5-day period. For SOD, the ~27- and ~ 13.5-day periods are the strongest up to the beginning of 2019. After that, a clear weakening in the power for both periods is observed. REA shows a strong common power around the 27-day period between 2007 and 2008, and during 2011–2017. For the ~13.5-day period, an increase in the power is clearly observed during 2011–2017. For CAS, the ~27- and ~13.5-day periods are stronger during 2012–2018 than at other time intervals. In general, Fig. 7 shows a strong common power between PG and neutron monitor data around the 27-day and 13.5-day periods for many of the PG measurement sites (at different time intervals). There are no significant 27 day period enhancements around 2010 and 2020 for all PG sites, which coincides with solar minimum times, when no solar co-rotating interaction regions (CIR) were present. In particular, the time interval of 2007–2008 involved a repetitive CIR, which has been reported previously by other authors (e.g. Harrison and Lockwood, 2020), and will be discussed in more detail below. It is important to note that different time windows are analysed for different sites, therefore different types of solar influences are present depending on the exact time interval. This will be further discussed in Section 6.

To investigate the time dependency of the 13.5- and 27-day periodicities at the various PG measurement sites, Fig. 8 plots the global XWT spectrum for the PG and neutron monitor data for two different time intervals of (a) increasing solar activity (i.e., as the sunspot increases towards solar maximum), and (b) decreasing solar activity (i.e., declining phase of solar cycle). Fig. 8 demonstrates a much stronger relationship between neutron monitor and PG data for the 27 day periodicity at all sites during declining phases of the solar cycle (Fig. 8b) than increasing phases (Fig. 8a). This is likely related to the more regular occurrence of coronal holes during periods of solar minimum. Coronal holes enhance the solar wind outflow and influence the formation of long-lived co-rotating interaction regions (CIRs), which are known to modulate galactic cosmic ray (GCR) fluxes. As CIRs are features on the solar surface that rotate with the sun approximately every 27 days, it follows that a characteristic 27 day oscillation is observed in GCR data (through neutron monitor measurements) (e.g., Harrison et al., 2011), and evidence of similar oscillatory periods has also been observed in surface atmospheric electricity measurements (e.g., Harrison et al., 2011, 2013). Known time intervals of strong CIR activity include solar

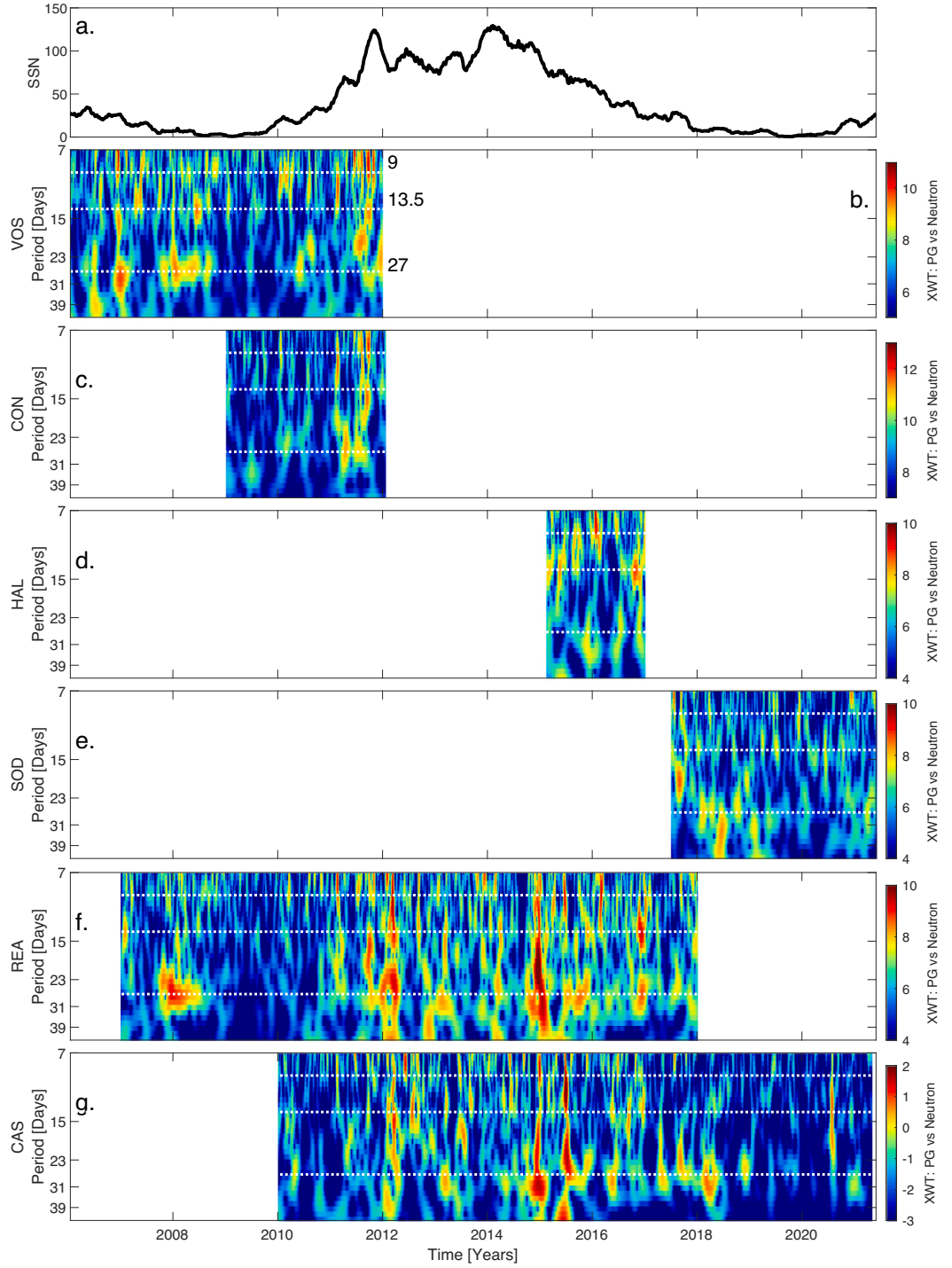

Fig. 7. (a) Temporal evolution of the sunspot number for solar cycle 24 with a 4 month moving average. XWT distribution between PG and cosmic-ray neutron variabilities for (b) VOS, (c) CON, (d) HAL, (e) SOD, (f) REA, and (g) CAS. The colour contours indicate the high (red) and low (blue) significant common powers of two wavelet transforms. Gaps (white colour) indicate no PG data record. Horizontal white lines indicate the 9-, 13.5- and 27-day periodicities. (For interpretation of the references to colour in this figure legend, the reader is referred to the web version of this article.)

minimum during 1996–1998 and 2007–2009 (Rouillard et al., 2007), with weaker events during 2014–2015 (Gil and Mursula, 2018) and from 2017 to 2018 (Ghanbari et al., 2019). From the two sites with PG data from 2007 to 2009 (VOS and REA), both exhibit strong relationships with neutron monitor data around the 27-day period (as shown in Fig. 7). CAS and REA show peaks at 27 days during the 2014–2015 event; and SOD for the 2017–2018 event (Fig. 7). We therefore conclude that CIR events during solar minimum are frequently observed in surface PG data from many sites ranging from mid latitudes to high latitudes.

In order to investigate whether the 27-day periodicities could be caused by local meteorological influences on the PG, rather than solar influences, meteorological data from all of the PG measurement sites (where available) was analysed. The XWT spectrum for PG vs temperature, pressure and wind direction for the various measurement sites, is plotted in Fig. 9, with the 27-day periodicity highlighted by the black horizontal line. Multiple data series on the same plot indicate the various

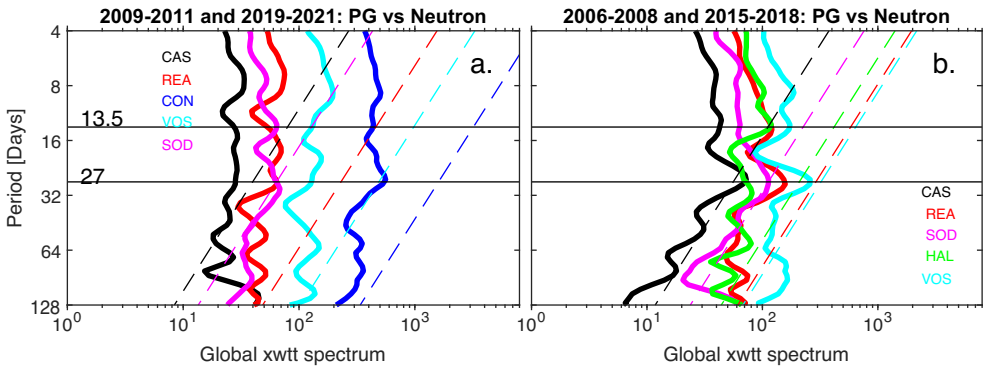

Fig. 8. Global XWT power spectrum between PG and cosmic-ray neutron time series for (a) the solar minima and increasing solar activity phase from 2009 to 2011 and 2019–2021 and (b) the declining phases of 2006–2008 and 2015–2018 (b). The result for each station (continuous) and their respective 95% confidence interval (dashed) are colour differentiated. Results for CAS are multiplied by a factor of 100 for visualisation comparison. The horizontal lines indicate the 13.5-day and 27-day periods.

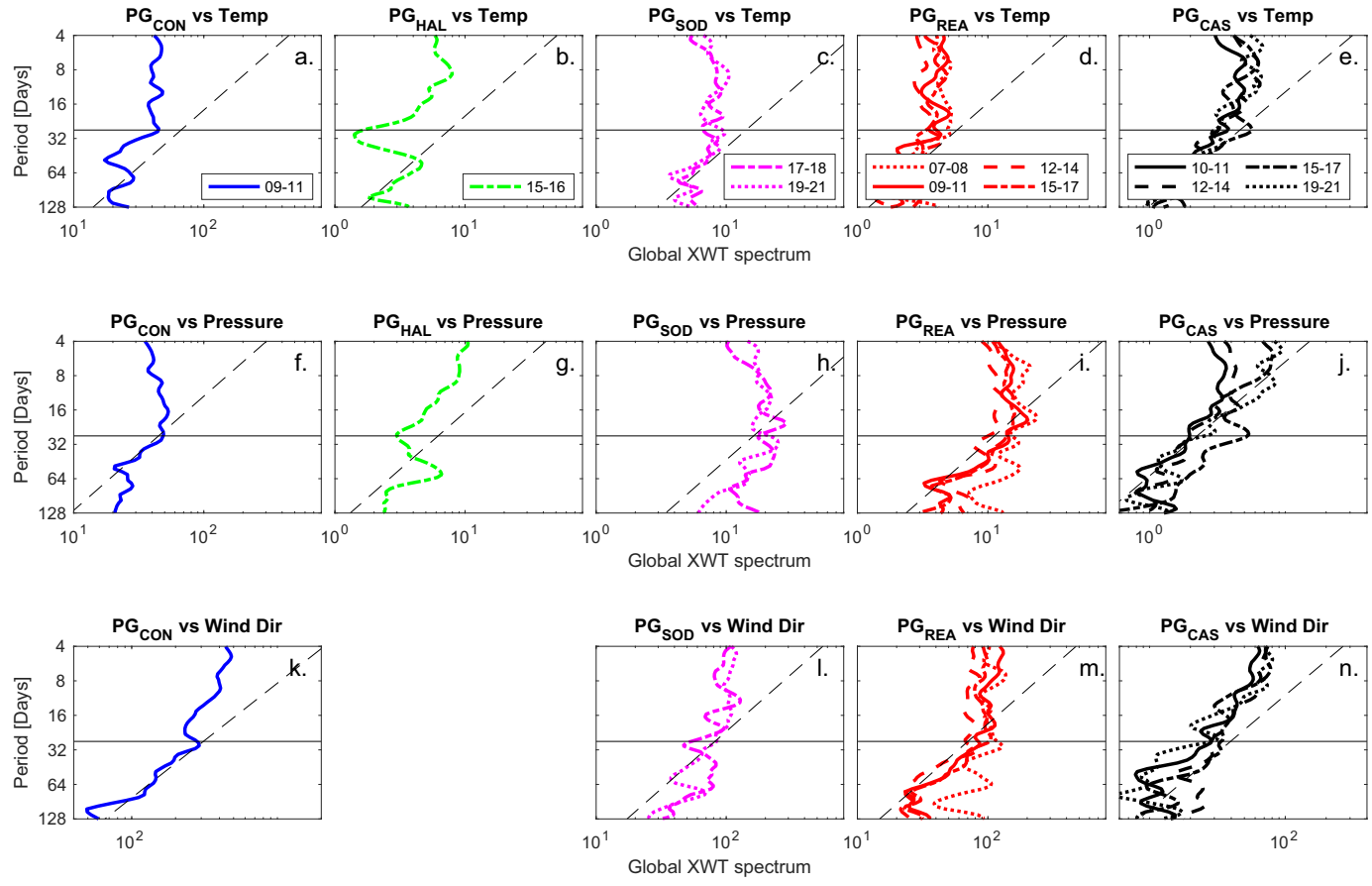

Fig. 9. Global XWT power spectrum between PG and meteorological time series, where each column (colour differentiated) corresponds to each of the stations: CON (c, f, k), HAL (b, g), SOD (c, h, l), REA (d, i, m), and CAS (e, j, n). The top, middle and bottom rows correspond to PG vs temperature, vs pressure, and vs wind direction, respectively. The different line styles identify the different analysed time windows within the time series. The horizontal black line marks the 27-day period. Dashed black lines indicate the 95% confidence interval.

measurement time windows analysed (e.g. for CAS, the years 2010–2013, 2013–2016; and 2016–2019 are analysed separately to provide a more consistent measurement period across all sites). There is no wind direction plot for Halley as this data was not available at the time of writing the paper. As can be seen in Fig. 9, there is no evidence of any strong correlation between PG and any of the examined meteorological variables on a 27-day timescale. In addition, we analysed the relation between PG versus meteorological parameters during the same time intervals as Fig. 8 (shown in the Fig. A1 in the Appendix) and still there is no evidence of a correlation for the 27-day period. These results suggest that the origin of the 27-day periodicity is not caused by local meteorological effects.

The origin of the 27-day period observed in atmospheric and electric parameters has also been associated with the Madden-Julian Oscillation (MJO) (e.g., Anyamba et al., 2000; Takahashi et al., 2010; Miyahara et al., 2017; Beggan and Musur, 2019). The MJO consists of large-scale coupled patterns in atmospheric circulation and deep convection, and is the dominant component of the intraseasonal variability in the tropical atmosphere. It propagates eastward across the equatorial Indian and western/central Pacific oceans and has a periodicity between 30 and 90 days (Zhang, 2005), with the most frequent period being ~45 days (Madden and Julian, 1994). The most popular index used for MJO prediction studies is the Real-time Multivariate MJO (RMM). RMM1 and RMM2 are the first and second principal components of the combined

empirical orthogonal functions of outgoing longwave radiation and zonal wind at different altitudes and latitudes. More details about the RMM indices can be found in Kim et al. (2018). We have calculated the periodicities of the RMM indices using the wavelet transform between 2006 and 2021. The results are shown in Fig. A2 in the Appendix. A broad peak is observed around 30–60 days with a maximum in 45 days for both indices. From Fig. 6 we observed PG periodicities between 44 and 52 days, highlighting the possibility of an influence of the MJO on

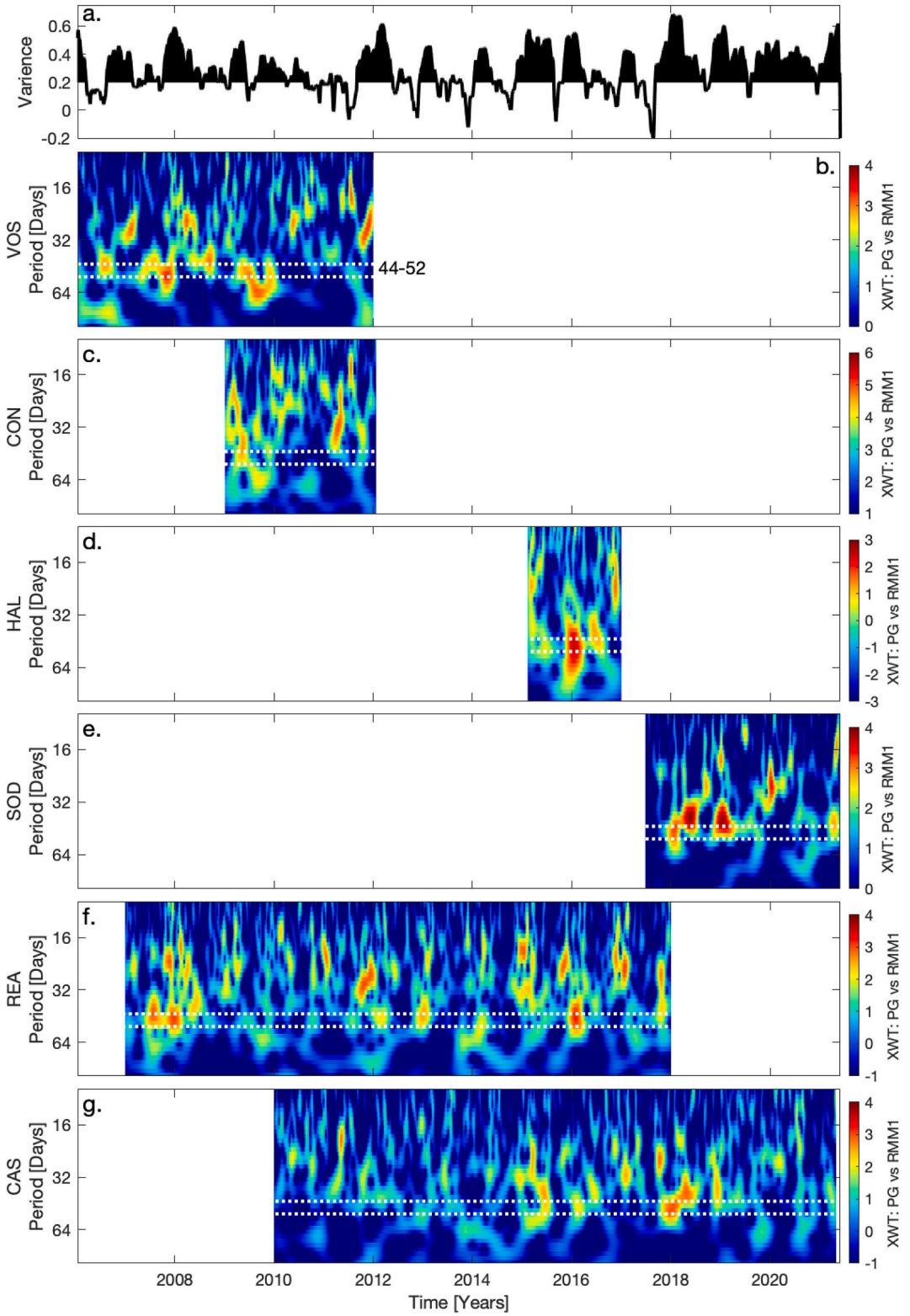

Fig. 10. (a) Temporal evolution of the logarithmic MJO variance (RMM1^2 + RMM2^2) after applying a 93-day moving average. XWT distribution between PG and RMM1 index for (b) VOS, (c) CON, (d) HAL, (e) SOD, (f) REA, and (g) CAS. The contour colors indicate the high (red) and low (blue) significant common powers of two wavelet transforms. Gaps (white colour) indicate no PG data record. Horizontal white lines indicate the 44–52 days periodicities. (For interpretation of the references to colour in this figure legend, the reader is referred to the web version of this article.)

the PG. To go further on this we performed the XWT between the PG versus the MJO indices (RMM1 and RMM2).

Fig. 10 shows in the top panel the logarithmic of the MJO variance (RMM1^2 + RMM2^2), applying a moving average with a time window of 93 days. The variance gives an indication of the intensity of the MJO (Wheeler and Hendon, 2004). The figure also shows the XWT distribution between PG and RMM1 index. In the latter, the colors indicate the common power of the two CWT examined, one for PG and the other for RMM1 index, ranging from low (blueish) to high (reddish). In Fig. 10, the XWT for VOS shows common power between 40-day and 60-day periods during 2006–2009. Similar behavior is observed for CON during 2009. For HAL, common powers between 35 and 65 days are observed throughout the time window and are particularly stronger around December 2016. For SOD, the periods between 35 and 60 days are the strongest during 2018 and the beginning of 2019. REA shows a strong common power between 35 and 60 days during 2007 and the beginning of 2008, and around December 2016. During 2012 and 2013, these periods were more intermittent. For CAS, common powers between 35 and 60 days are stronger around December 2015 and December 2018. For all stations, common power periods between 16 and 32 days are less frequent.

We go further on the possibility of the 27-day period being a harmonic of the MJO, thus, Fig. 11 shows the Global XWT power spectrum between PG and RMM1 index during the same time intervals of Fig. 8 for comparison. There is no evidence of a strong power of the 27-day period in both time intervals. Instead, the common power is more intense between 32 and 64 day, with a maximum at ~45-day period clearly observed at HAL, VOS, SOD, and REA sites during the declining phase of the solar cycle (Fig. 11b). Similar results are found for XWT and Global XWT between PG versus RMM2 index (not shown here).

6. Discussion

This study shows the spectral analysis of the PG variation for different sites. The sites are located in high and middle-latitude in the Northern and Southern hemispheres. We performed the Lomb-Scargle and the wavelet transform techniques to calculate the main PG periodicities. The 0.5-, 1-, ~27-, ~45-, ~180- and 365-day periods are observed for almost all sites independently of their location (e.g., latitude, altitude).

The origin of the 0.5-, 1-, ~180- and 365-day periods observed in the PG variation are associated with the GEC behavior and/or local effects as mentioned in section 4.1 and 4.3. The comparable prominence for the 0.5- and 1-day period observed during June, July and August for VOS, CON, and HAL sites, in combination with the fact that these sites are very clean, strongly suggests that the 0.5-day period is a representation of the GEC behavior. PG daily curves presented two main peaks at ~09 and ~19UT, which are also observed in the Carnegie daily curve (Harrison, 2013) and the thunderstorm global daily curve (Anca et al., 2021) for JJA months. These peaks correspond to the Australian/Asian and American convective activity, respectively, supporting the statement that this period is associated with the GEC behavior. For SOD, REA and CAS sites, which are semi-urban, urban and mountain-region sites, respectively, the peak observed at 09UT (GEC behavior) could present an enhancement (REA, SOD) or suppression (CAS) due to local effects (e.g., pollution, sunrise effect) affecting this periodicity.

Evidence of the 27-day period on PG has been previously reported (Harrison et al., 2011; Harrison et al., 2013; Chum et al., 2021), and its origin may be associated with the solar rotation period. The mechanisms involved about how the solar rotation modulates the PG are, however, not straightforward. Previous studies reported that solar energetic particles from the Sun modulate the galactic cosmic radiation and this modulation produces changes in the PG and Jc (air-Earth current density) in fair-weather regions, at different time scales, through the GEC (Markson, 1978; Markson and Muir, 1980; Markson, 1981; Farrell and Desch, 2002). On a long-term scale, Harrison and Usoskin (2010) reported a variation of 12% (in PG) and 16.5% (in Jc) in electrical parameters, associated with a ~ 8% variation in NM data during the transition between cosmic ray maximum and minimum (corresponding to the solar cycle 21). About the 27-day variation observed in cosmic rays, it has been discussed that the main source of this modulation is the passage of Corotating interaction regions (CIR) (Simpson, 1998; Richardson, 2004 and references therein). In this way, Harrison et al. (2011) and Harrison et al. (2013) reported a 27-day period in PG measurements during the passages of two different CIR that occurred during 1996–1997 and 2007–2009, respectively, recorded at two different mid-latitude stations. It is worth taking in consideration that different lengths of datasets analysed at different times mean that we may not be observing the same physical influences in each dataset (especially solar influences, which can occur only during certain time periods as discussed in section 5). Nevertheless, from Fig. 7, even using different time windows for different stages of the solar cycle, a solar influence can be observed in all stations and also its solar cycle dependence. For instance, the results of this study showed that strong common power between PG and cosmic rays (NM data) in the 27-day period appears during the passage of different CIR events: september 2007-June 2008 (Gil and Mursula, 2018) observed at VOS and REA (also previously reported by Harrison et al., 2013), August 2014–March 2015 (Gil and Mursula, 2018) observed at REA and CAS, 2017–2018 (Ghanbari et al., 2019) observed at SOD and CAS. Furthermore, from Fig. 8b the 27-day period is clearly seen during the declining phase-minima of the solar cycle (period where CIR are more recurrent) compared with the minima-increasing phase (Fig. 8a). It is worth pointing out that the 27-day period appears in all stations from high to middle latitudes, during

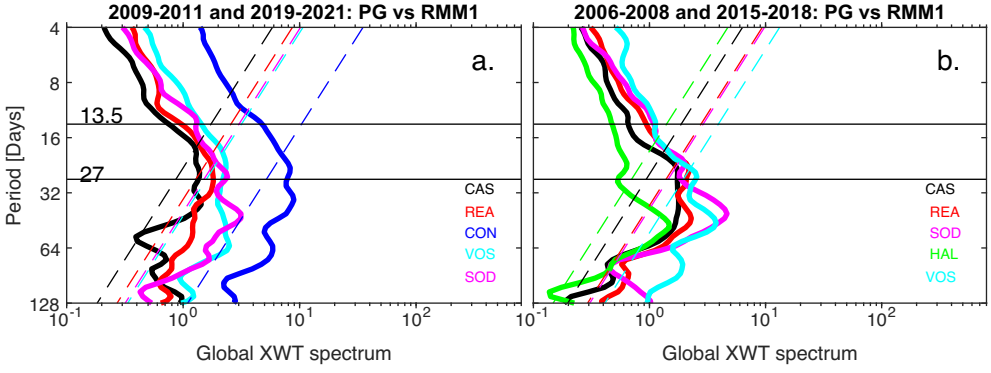

Fig. 11. Global XWT power spectrum between PG and RMM1 index for the same time windows as Fig. 8 (a) 2009–2011 and 2019–2021 and (b) 2006–2008 and 2015–2018 (b). The result for each station (continuous) and their respective 95% confidence interval (dashed) are colour differentiated. The horizontal lines indicate the 13.5-day and 27-day periods.

the passages of the CIR events. However, we are not able to discern if the 27-day period signals are stronger at any specific latitude, since a direct comparison between XWT of the different stations is not possible here.

The origin of the 27-day periodicity has also been associated with the MJO oscillation (e.g., Anyamba et al., 2000). However, from Figs. 10 and 11 we found that there are just intermittent (if any) common powers between the PG and MJO indices at this period. Instead, there are strong common powers between 30 and 60-days, which are characteristic periods of the MJO (Madden and Julian, 1994). The mechanism is straightforward, since the MJO modulates the GEC by varying the thunderstorm and electrified shower cloud activity, and therefore the PG. Peterson et al. (2017) reported that the MJO produces a variability of 14% on the GEC current, therefore producing changes in the electrical parameters in fair weather regions. It is worth noting that the common powers are stronger during some years and totally suppressed during others. This could be associated with variations in the intensity of the MJO (which is shown in the top panel of Fig. 10). For example, around December 2017–January 2018 the intensity of the MJO is stronger and we observe a strong common power at SOD and CAS sites. Another possibility could be associated with El Nino - Southern Oscillation (ENSO). Some studies reported the interrelationship between the MJO teleconnections and ENSO via constructive and destructive interference of the MJO and ENSO signals (Arcodia et al., 2020). During December 2015–January 2016 a stronger El Nino was reported, which coincides with a strong common power around this time interval at HAL and REA sites. From Fig. 11, there is another important point to highlight, in that during the declining phase of the solar cycle there is a single maximum observed at ~45-day in the PG periods (except for CAS) compared with the rising phase, where there is a broader peak. It could be just the case that the 45-day period was more predominant during these time intervals, however, a solar influence should not be discarded since several studies have reported a solar influence on the MJO activity (Djurovic et al., 1994; Blanter et al., 2012; Hood, 2018; Le Mouel et al., 2019; Hoffmann and von Savigny, 2019). It is important to point out that in this work we only used the RMM index as indication of the MJO activity. Further research should include other MJO indices, but this is beyond the scope of this paper.

7. Conclusions

This paper presents the first comprehensive spectral analysis of near surface PG data from multiple measurement sites at a variety of geographical latitudes ranging from polar regions to mid latitude sites. All of the selected sites have shown evidence of Global Electric Circuit (GEC) influences in previous studies. We employ a variety of spectral techniques including Lomb-Scargle periodograms (LSP) to study the power spectra of the data, as well as cross-wavelet transforms (XWT) in order to compare different parameters such as PG and neutron monitor data to study solar influences. Periodograms of PG data show that 0.5- and 1-day periodicities dominate at all sites (Vostok, Concordia, and Halley in Antarctica; Sodankyla in the Arctic, and Reading and Casleo in mid latitude regions). This results from a combination of local meteorological factors (which are primarily responsible for the 0.5-day peak in Reading), and global influences from the GEC. Seasonal analysis of LSPs for PG data showed that the 0.5-day (1-day) period is more predominant during June–July-August (December–January-February) months. This provides valuable information about the strength of local influences at a site versus GEC ones. This work also demonstrates that significant periodicities are also observed for the 365- and 180-day periodicity at most sites (due to the annual cycle in the GEC as well as local meteorological influences). Evidence of 44–52 day periodicities are present at Sodankyla and Halley, which show similarities with the peak periodicity of 45 days from the Madden-Julian Oscillation (MJO). It is therefore possible that changes in the circulation in the equatorial Indian and western/central Pacific ocean have an observable effect on surface atmospheric electricity measurements in the polar regions.

The LSPs and XWT performed here also demonstrate evidence of solar periodicities in the PG data at 9-, 13.5- and 27-day. In particular, XWT demonstrates strong similarities in the power spectra between PG and neutron monitor data (used here as a proxy for Galactic Cosmic Ray ionisation) during periods of declining solar activity and solar minimum. Many of these periods correspond to known incidences of solar coronal holes, which generate Co-rotating Interaction Regions (CIRs), and produce strong 27-day oscillations in neutron monitor data. The analysis here shows that such CIR periods are often observed in surface PG data ranging from mid latitude to high latitude sites, which demonstrates a strong influence of solar activity on atmospheric electricity during certain time intervals. This paper therefore demonstrates the usefulness of spectral analysis techniques to study local and global influences on atmospheric electricity in order to understand more about the physical processes affecting Earth's electrical environment.

Declaration of Competing Interest

None.

Acknowledgements

KAN acknowledges an Independent Research Fellowship funded by the Natural Environment Research Council (NERC) (NE/L011514/1 and NE/L011514/2). JT acknowledges the Polish National Agency for Academic Exchange for funding of the Ulam Program scholarship agreement no PPN/ULM/2019/1/00328/U/00001.

Data availability

- Sodankyla PG data are available from KN (k.a.nicoll@reading.ac.uk) at the University of Reading on request. Reading, CAS and Halley PG data is available from the GloCAEM database: http://data.ceda.ac.uk/badc/glocaem/data/. Sodankyla meteorological data is available from the LITB database of the Finnish Meteorological Institute(https://litdb.fmi.fi/).
- Vostok PG from: Burns, G., Tinsley, B., Frank-Kamenetsky, A.V., Troshichev, O. and Bering, E.A. (2013) Vertical electric field - Vostok from 2006 to 2011, Ver. 2, *Australian Antarctic Data Centre* - doi: https://doi.org/10.4225/15/58880fc1a1fbd.
- Concordia PG from: Burns, G., Troshichev, O., Tinsley, B., Bering, E. A. and Symons, L. (2013) Vertical Electric Field data from Concordia Station - 2009 - 2012, Ver. 1, *Australian Antarctic Data Centre* - doi: https://doi.org/10.4225/15/5875ad6740e93.
- Concordia meteorological data were obtained from "Meteo-Climatological Observatory" of PNRA (www.climantartide.it).
- CAS meteo data is available from https://casleo.conicet.gov.ar/datos-utiles/.
- Sunspot number data were obtained from https://omniweb.gsfc.nasa.gov/form/dx1.html
- Oulu and Athens neutron monitor data were obtained from https://www.nmdb.eu/nest/ McMurdo NM data is available from http://cr0.izmiran.ru/mcmd/main.htm
- MJO indices (RMM1 and RMM2) are available from http://www.bom.gov.au/climate/mjo/

Appendix A

Fig. A1 shows the global XWT spectrum for the PG and meteorological parameters (temperature, wind direction and pressure) for the same intervals indicated in Fig. 8 (Left: increasing solar activity, Right: decreasing solar activity). There is no evidence of strong common power for the 27-day period for all sites.

Fig. A2 shows the wavelet analysis for the MJO indices: RMM1 (a,b,c) and RMM2 (d,e,f). (a,d) Time series, where few data gaps were filled using a moving average of the original time series. (b,e) The continuous wavelet power spectra corrected by their scales (Liu et al., 2007). (c,f) The global wavelet power spectra. The dashed line represents the 98% confidence level for a red noise background level. The black horizontal line indicates the maximum period.

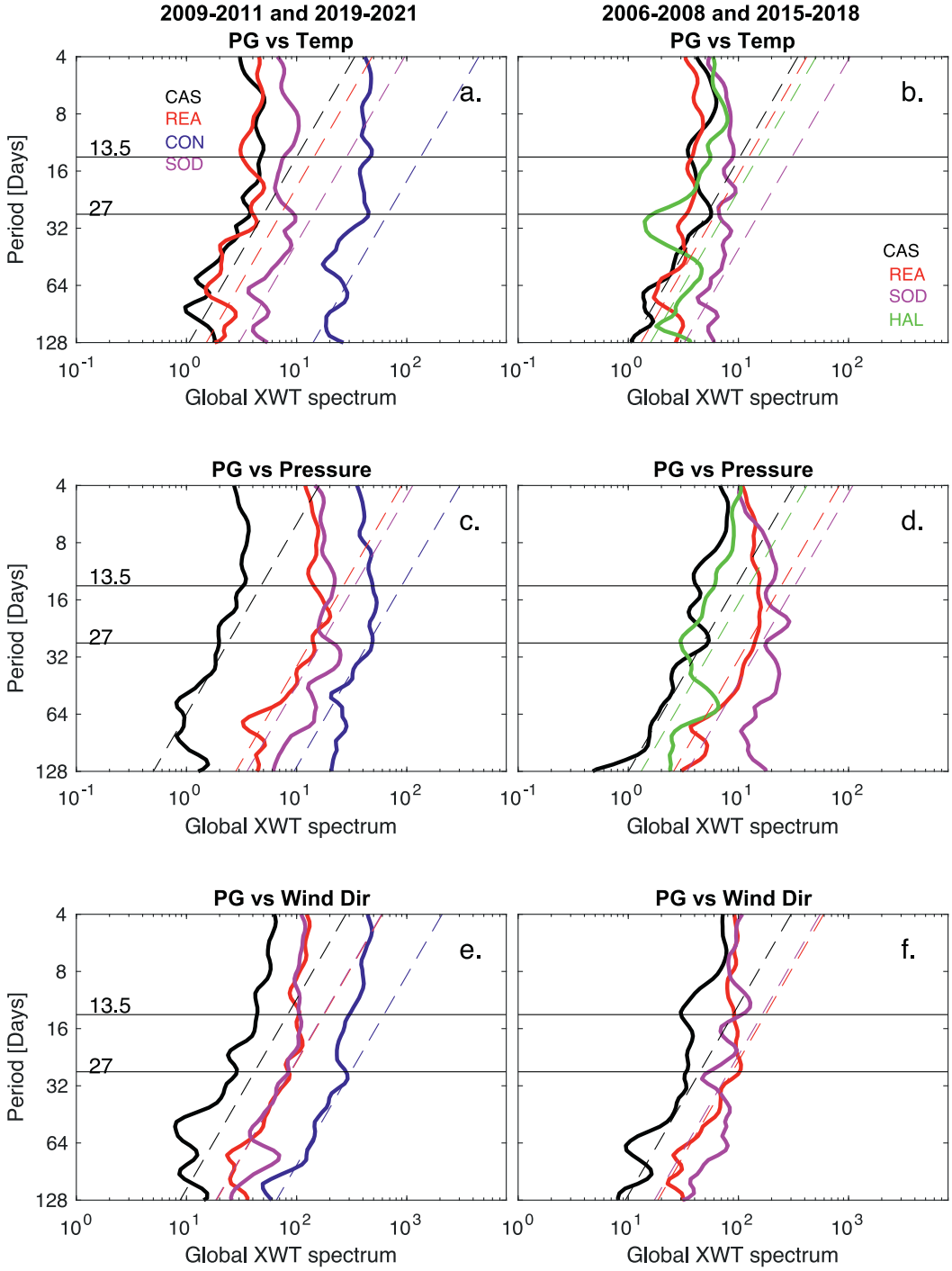

Fig. A1. Global XWT power spectrum between PG and meteorological time series for the solar minima of 2009–2011 and 2019–2021 (left) and the declining phases of 2006–2008 and 2015–2018 (right). The top (a, b), middle (c, d), and bottom (e, f) panels are the Global XWT power spectrum of PG with temperature, PG with pressure, and PG with wind direction, respectively. The result for each station (continuous) and their respective 95% confidence interval (dashed) are colour differentiated. The horizontal lines indicate the 13.5-day and 27-day periods.

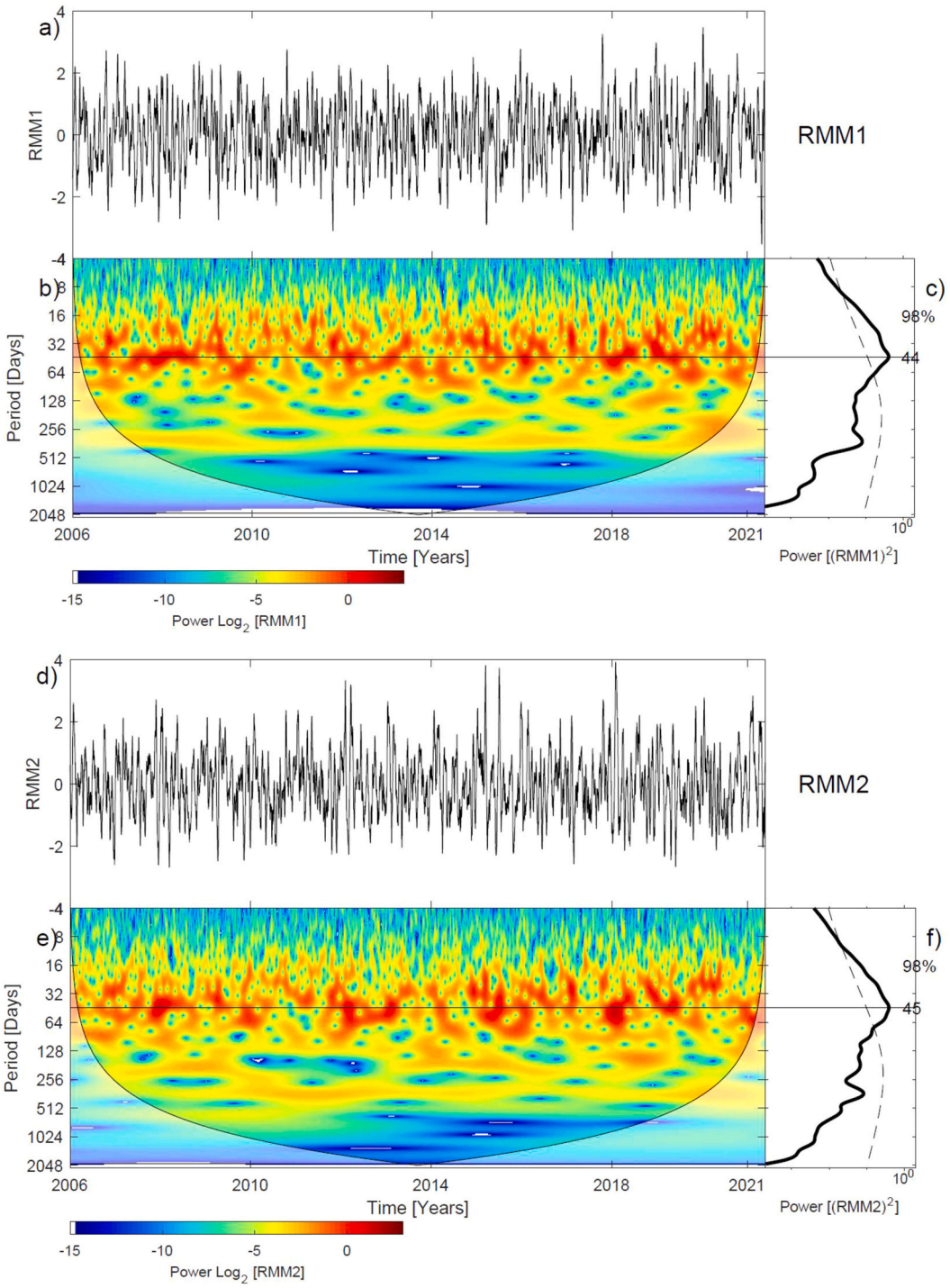

Fig. A2. Wavelet analysis for MJO indices (RMM1, top panel, and RMM2, bottom panel). For each RMM index the daily average is shown (a,d). (b,e) Contours in the time–period domain of the real part of the wavelet power spectra of the RMM index. The contour colors indicate the minimum and maximum magnitude, from blue to red, of the matches between the phases of the time series and the wavelet. The white shadowed lateral edges are values within the cone of influence. (c,f) The global wavelet power spectrum. The horizontal lines indicate the most significant oscillations and the dashed curve is the 98% confidence. (For interpretation of the references to colour in this figure legend, the reader is referred to the web version of this article.)

References

Aich, V., Holzworth, R., Goodman, S.J., Kuleshov, Y., Price, C., Williams, E., 2018. Lightning: a new essential climate variable. Eos 99. https://doi.org/10.1029/2018EO104583.

Anca, J.G., Tacza, J., Raulin, J.-R., Morales, C.A., 2021. Estimation of thunderstorms occurrence from lightning cluster recorded by WWLLN and its comparison with the 'universal' Carnegie curve. J. Atmos. Sol. Terr. Phys. 221, 105682.

Anisimov, S.V., Mareev, E.A., Shikhova, N.M., Dmitriev, E.M., 2002. Universal spectra of electric field pulsations in the atmosphere. Geophys. Res. Lett. 29 (24), 2217.

Anisimov, S.V., Afinogenov, K.V., Shikhova, N.M., 2014. Dynamics of undisturbed midlatitude atmospheric electricity: from observations to scaling. Radiophysics and Quantum Electronics 56 (11–12), 709–722.

Anyamba, E., Williams, E., Susskind, J., Fraser-Smith, A., Fullekrug, M., 2000. The manifestation of the Madden-Julian Oscillation in global deep convection and in the Schumann Resonance intensity. J. Atmos. Sci. 57, 1029–1044.

Arcodia, M.C., Kirtman, B.P., Siquiera, L.S., 2020. How MJO teleconnections and ENSO interference impacts U.S. Precipitation. Journal of Climate 33 (11), 4621–4640.
Bazilevskaya, G.A., Usoskin, I.G., Fluckiger, E.O., Harrison, R.G., Desorgher, L., Butikofer, R., Krainev, M.B., Makhmutov, V.S., Stozhkov, Y.I., Svirzhevskaya, A.K., Svirzhevsky, N.S., Kovaltsov, G.A., 2008. Cosmic rays induced ion production in the atmosphere. Space Sci. Rev. 137 (1–4), 149–173.
Beggan, C.D., Musur, M., 2019. Is the Madden-Julian Oscillation reliably detectable in Schumann Resonances? J. Atmos. Sol. Terr. Phys. 190, 108–116.
Blanter, E., Le Mouel, J.-L., Shnirman, M., Courtillot, V., 2012. A correlation of mean period of MJO índices and 11-yr solar variation. J. Atmos. Sol. Terr. Phys. 80, 195–207.
Burns, G.B., Frank-Kamenetski, A.V., Troshichev, O.A., Bering, E.A., Redell, B.D., 2005. Interannual consistency of bi-monthly differences in diurnal variations of the ground-level, vertical electric field. J. Geophys. Res. 110 (D10), 106.
Burns, G.B., Tinsley, B.A., Frank-Kamenetski, A.V., Troshichev, O.A., French, W.J.R., Klekociuk, A.R., 2012. Monthly diurnal global atmospheric circuit estimates derived from Vostok electric field measurements adjusted for local meteorological and solar wind influences. J. Atmos. Sci. 69 (6), 2061–2082.
Burns, G.B., Frank-Kamenetski, A.V., Tinsley, B.A., French, W.J.R., Grigioni, P., Camporeale, G., Bering, E.A., 2017. Atmospheric global circuit variations from vostok and concordia electric field measurements. J. Atmos. Sci. 74 (3), 783–800.
Chum, J., Kollárik, M., Kolmasová, I., Langer, R., Rusz, J., Saxonbergová, D., Strhárský, I., 2021. Influence of Solar Wind on secondary Cosmic Rays and Atmospheric Electricity. Front. Earth Sci. 9, 671801.
Conceição, R., Silva, H.G., Bennett, A., Salgado, R., Bortoli, D., Costa, M.J., Pereira, M.C., 2018. High-frequency response of the atmospheric electric potential gradient under strong and dry boundary-layer convection. Bound.-Layer Meteorol. 166 (1), 69–81.
Djurovic, D., Paquet, P., Billiau, A., 1994. New indications for the solar origin of the 50-day cycle in the atmospheric circulation and Earth's rotation. Astron. Astrophys. 288, 335–341.
Farrell, W.M., Desch, M.D., 2002. Solar proton events and the fair weather field at ground. Geophys. Res. Lett. 29 (9), 1323.
Ghanbari, K., Florinski, V., Guo, X., Hu, Q., Leske, R., 2019. Galactic cosmic rays modulation in the vicinity of corotating interactions regions: observation during the last two solar minima. Astrophys. J. 882, 54.
Gil, A., Mursula, K., 2018. Comparing two intervals of exceptionally strong solar rotation recurrence of galactic cosmic rays. J. Geophys. Res. Space Physics 123 (8), 6148–6160.
Grinsted, A., Moore, J.C., Jevrejeva, S., 2004. Application of the cross wavelet transform and wavelet coherence to geophysical time series. Nonlinear Process. Geophys. 11, 561–566. https://doi.org/10.5194/npg-11-561-2004.
Gurgenashvili, E., Zaqarashvili, T.V., Kukhianidze, V., Oliver, R., Ballester, J.L., Ramishvili, G., Shergelashvili, B., Hanslmeier, A., Poedts, S., 2016. Rieger-type periodicity during solar cycles 14-24: Estimation of dynamo magnetic field strength in the solar interior. Astrophys. J. 826, 55.
Harrison, R.G., 2013. The Carnegie curve. Surv. Geophys. 34 (2), 209–232.
Harrison, R.G., Lockwood, M., 2020. Rapid indirect solar responses observed in the lower atmosphere. Proceeding of the Royal Society A 476, 20200164.
Harrison, R.G., Märcz, F., 2007. Heliospheric timescale identified in surface atmospheric electricity. Geophys. Res. Lett. 34 (23).
Harrison, R.G., Nicoll, K.A., 2018. Fair weather criteria for atmospheric electricity measurements. Journal of Atmospheric and Solar Terrestrial Physics 179, 239–250.
Harrison, R.G., Usoskin, I., 2010. Solar modulation in surface atmospheric electricity. Journal of Atmospheric and Solar Terrestrial Physics 72, 176–182.
Harrison, R.G., Ambaum, M.H.P., Lockwood, M., 2011. Cloud base height and cosmic rays. Proceeding of the Royal Society A 467, 2777–2791.
Harrison, R.G., Nicoll, K.A., McWilliams, K.A., 2013. Space weather driven changes in lower atmosphere phenomena. J. Atmos. Sol. Terr. Phys. 98, 22–30.
Harrison, R.G., Nioll, K.A., Aplin, K., 2014. Vertical profile measurements of lower troposphere ionization. J. Atmos. Sol. Terr. Phys. 119, 203–210.
Harrison, R.G., Nicoll, K.A., Mareev, E., Slyunyaev, N., Rycroft, M.J., 2020. Extensive layer clouds in the global electric circuit: their effects on vertical charge distribution and storage. Proceeding of the Royal Society A 476, 20190758.
Hoffmann, C.G., von Savigny, C., 2019. Indication for a potential synchronization between the phase evolution of the Madden-Julian oscillation and the solar 27-day cycle. Atmos. Chem. Phys. 19, 4235–4256.
Holzworth, R.H., Brundell, J.B., McCarthy, M.P., Anderson, T.S., 2021. Lightning in the Arctic. Geophys. Res. Lett. 48 (e2020GL091366).
Hood, L.L., 2018. Shor-term solar modulation of the Madden-Julian climate Oscillation. J. Atmos. Sci. 75 (3), 857–873.
Israelsson, S., Oluwafemi, C., 1975. Power and cross-power spectral studies of electric and meteorological parameters under fair weather conditions in the atmospheric surface layer. Bound.-Layer Meteorol. 9 (4), 461–477.
Jeong, J., Oh, S., 2022. Seasonal trends of the cosmic ray intensity observed by 16 neutron monitors for 1964-2020. Advances in Space Research. https://doi.org/10.1016/j.asr.2022.02.052 in press.
Kato, C., Munakata, K., Yasue, S., Inoue, K., McDonald, F.B., 2003. A 1.7-year quasi-periodicity in cosmic ray intensity variation observed in the outer heliosphere. J. Geophys. Res. 108 (A10), 1367. https://doi.org/10.1029/2003JA00989.
Kim, H., Vitart, F., Waliser, D.E., 2018. Prediction of the Madden-Julian Oscillation: a review. J. Clim. 31 (23), 9425–9443.
Le Mouel, J.-L., Lopes, F., Courtillot, V., 2019. A solar signature in many climate indices. Journal of Geophysical Research: Atmospheres 124, 2600–2619.
Liu, Y., San Liang, X., Weisberg, R.H., 2007. Rectification of the Bias in the Wavelet Power Spectrum. J. Atmos. Ocean. Technol. 24 (12), 2093–2102. https://doi.org/10.1175/2007JTECHO511.1.
Lomb, N.R., 1976. Least-squares frequency analysis of unequally spaced data. Astrophys. Space Sc. 39, 447–462. https://doi.org/10.1007/BF00648343.
Macotela, E.L., Clilverd, M., Manninen, J., Moffat-Griffin, T., Newnham, D.A., Raita, T., Rodger, C.J., 2019. D-region high-latitude forcing factors. J. Geophys. Res. Space Phys. 124, 765–781. https://doi.org/10.1029/2018JA026049.
Madden, R.A., Julian, P.R., 1994. Observations of the 40-50 day tropical oscillation - a review. Mon. Weather Rev. 122, 814–837.
Makhdoomi, B.A., Raina, B.N., 1988. Correlation and spectral analysis of atmospheric electric parameters. In: 8th International Conference on Atmospheric Electricity, pp. 130–137.
Markson, R., 1978. Solar modulation of atmospheric electrification and possible implications for the sun-weather relationship. Nature 273, 103–109.
Markson, R., 1981. Modulation of the Earth's electric field by cosmic radiation. Nature 291, 304–308.
Markson, R., Muir, M., 1980. Solar wind control of the Earth's electric field. Science 208, 979–990.
Mikhailov, Y.M., Mikhailova, G.A., Kapustina, O.V., Buzevich, A.V., Smirnov, S.E., 2004. Power spectrum features of the near-Earth atmospheric electric field in Kamchatka. Ann. Geophys. 47 (1).
Miyahara, H., Higuchi, C., Terasawa, T., Kataoka, R., Sato, M., Takahashi, Y., 2017. Solar 27-day rotational period detected in wide-area lightning activity in Japan. Ann. Geophys. 35, 583–588.
Morlet, J., Arens, G., Fourgeau, E., Glard, D., 1982. Wave propagation and sampling theory—part I: complex signal and scattering in multilayered media. Geophysics 47 (2), 203–221. https://doi.org/10.1190/1.1441328.
Nicoll, K.A., Harrison, R.G., 2016. Stratiform cloud electrification: comparison of theory with multiple in-cloud measurements. Q. J. R. Meteorol. Soc. 142 (700), 2679–2691.
Nicoll, K.A., Harrison, R.G., Barta, V., Bor, J., Brugge, R., Chillingarian, A., Chum, J., Georgoulias, A.K., Guha, A., Kourtidis, K., Kubicki, M., Mareev, E., Matthews, J., Mkrtchyan, H., Odzimek, A., Raulin, J.-R., Robert, D., Silva, H.G., Tacza, J., Yair, Y., Yaniv, R., 2019. A global atmospheric electricity monitoring network for climate and geophysical research. Journal of Atmospheric and Solar Terrestrial Physics 184, 18–29.
Oluwafemi, C.O., Ungethüm, E., Israelsson, S., Knudsen, E., 1974. Correlation and spectrum properties of the potential gradient and space-charge density in the atmospheric surface layer. Pure and Applied Geophysics 112 (3), 533–543.
Peterson, M., Deierling, W., Liu, Ch., Mach, D., Kalb, Ch., 2017. A TRMM/GPM retrieval of the total generator current for the global electric circuit. Journal Geophysical Research-Atmosphere 122, 10025–10049.
Press, W.H., Rybicki, G.B., 1989. Fast algorithm for spectral analysis of unevenly sampled data. Astrophys. J. 338, 277–280.
Price, C., 2009. Thunderstorms, Lightning and climate Change. In: Betz, H.D., Schumann, U., Laroche, P. (Eds.), Lightning: Principles, Instruments and Applications. Springer, Dordrecht.
Regener, E., Pfotzer, G., 1935. Vertical intensity of cosmic rays by threefold coincidences in the stratosphere. Nature 136, 718–719.
Richardson, I., 2004. Energetic particles and corotating interaction regions in the solar wind. Space Sci. Rev. 111, 267–376.
Rieger, E., Share, G.H., Forrest, D.J., Kanbach, G., Reppin, C., Chupp, E.L., 1984. A 154-day periodicity in the occurrence of hard solar flares? Nature 312 (5995), 623–625.
Rouillard, A.P., Lockwood, M., Finch, I., 2007. Centennial changes in the solar wind speed and in the open solar flux. J. Geophys. Res. Space Physics 112 (A5).
Sabbah, I., Kudela, K., 2011. Third harmonic of the 27 day periodicity of galactic cosmic rays: coupling with interplanetary parameters. Journal Geophysical Research Space Physics 116 (A4), A04103. https://doi.org/10.1029/2010ja015922.
Scargle, J.D., 1982. Studies in astronomical time series analysis. II- Statistical aspects of spectral analysis of unevenly spaced data. Astrophys. J. 263, 835–853.
Silva, H.G., Lopes, I., 2017. Rieger-type periodicities on the Sun and the Earth during solar cycles 21 and 22. Astrophysics and Space Science 362, 44.
Silva, H.G., Conceição, R., Melgão, M., Nicoll, K., Mendes, P.B., Tlemçani, M., Reis, A.H., Harrison, R.G., 2014. Atmospheric electric field measurements in urban environment and the pollutant aerosol weekly dependence. Environ. Res. Lett. 9 (11), 114025.
Silva, H.G., Lopes, F.M., Pereira, S., Nicoll, K., Barbosa, S.M., Conceição, R., Neves, S., Harrison, R.G., Pereira, M.C., 2016. Saharan dust electrification perceived by a triangle of atmospheric electricity stations in Southern Portugal. J. Electrost. 84, 106–120.
Simpson, J.A., 1998. A brief history of recurrent solar modulation of the galactic cosmic rays (1937-1990). Space Sci. Rev. 83, 169–176.
Singh, Y.P., Gautam, S., Badruddin, 2012. Temporal variations of short-and mid-term periodicities in solar wind parameters and cosmic ray intensity. J. Atmos. Sol. Terr. Phys. 89, 48–53. https://doi.org/10.1016/j.jastp.2012.07.011.
Stenflo, J.O., 1990. Time invariance of the sun's rotation rate. Astron. Astrophys. 233, 220–228.
Tacza, J., Raulin, J.P., Morales, C.A., Macotela, E., Marun, A., Fernandez, G., 2021a. Analysis of long-term potential gradient variations measured in the Argentinian Andes. Atmos. Res. 248, 105200.
Tacza, J., Nicoll, K.A., Macotela, E., Kubicki, M., Odzimek, A., Manninen, J., 2021b. Measuring global signals in the potential gradient at high latitude sites. Front. Earth Sci. 8, 614639.
Takahashi, Y., Okazaki, Y., Sato, M., Miyahara, H., Sakanoi, K., Hong, P.K., Hoshino, N., 2010. 27-day variation in cloud amount in the Western Pacific warm pool region and relationship to the solar cycle. Atmos. Chem. Phys. 10, 1577–1584.
Tinsley, B.A., 2008. The global atmospheric electric circuit and its effects on cloud microphysics. Rep. Prog. Phys. 71 (6), 066801.

Torrence, C., Compo, G., 1998. A practical guide to wavelet analysis. Bulletin of American Meteorological Society 79, 61–78.
Trevitt, A.C., 1984. Atmospheric electric modulation during a sea breeze. Journal of Geophysical Research: Atmospheres 89 (D6), 9663–9667.
Wheeler, M.C., Hendon, H.H., 2004. An all-season real-time multivariate MJO Index: Development of an Index for monitoring and Prediction. Mon. Weather Rev. 132 (8), 1917–1932.
Wilson, C.T.R., 1921. Investigations on lightning discharges and the electric field of thunderstorms. Philos Trans A 221, 73–115.
Xu, B., Zou, D., Chen, B.Y., Zhang, J.Y., Xu, G.W., 2013. Periodic variations of atmospheric electric field on fair weather conditions at YBJ, Tibet. Journal of Atmospheric and Solar-Terrestrial Physics 97, 85–90.
Zhang, C., 2005. Madden-Julian Oscillation. Rev. Geophys. 43, RG2003.